Chemical Engineering Journal 450 (2022) 138082

Contents lists available at ScienceDirect

Chemical Engineering Journal

journal homepage: www.elsevier.com/locate/cej

Immobilized N-C/Co derived from ZIF-67 as PS-AOP catalyst for effective tetracycline matrix elimination: From batch to continuous process

Xiu-Wu Zhang [a,b], Ming-Yan Lan [a,b], Fei Wang [a,b], Chong-Chen Wang [a,b,*], Peng Wang [a,b], Chengjun Ge [c], Wen Liu [d]

[a] Beijing Key Laboratory of Functional Materials for Building Structure and Environment Remediation, Beijing University of Civil Engineering and Architecture, Beijing, 100044, China
[b] Beijing Energy Conservation & Sustainable Urban and Rural Development Provincial and Ministry Co-construction Collaboration Innovation Center, Beijing University of Civil Engineering and Architecture, Beijing 100044, China
[c] Key Laboratory of Agro-Forestry Environmental Processes and Ecological Regulation of Hainan Province, School of Ecology and Environment, Hainan University, Haikou 570228, China
[d] College of Environmental Sciences and Engineering, Peking University, The Key Laboratory of Water and Sediment Sciences, Ministry of Education, Beijing 100871, China

ARTICLE INFO

Keywords:
ZIF-67
Derivatization
Immobilization
Advanced oxidation processes
Wastewater remediation

ABSTRACT

The successful preparation of immobilized nitrogen-doped carbon/cobalt @ porous spherical substrate (N-C/Co@PSS) catalyst derived from ZIF-67 was reported in this work. The oxytetracycline (OTC), tetracycline (TTC), and chlortetracycline (CTC) in the simulated wastewater were decomposed via the peroxymonosulfate (PMS) activation by N-C/Co@PSS. The degradation of TCs was initially investigated by batch-type experiments, in which ca. 100% TCs with an initial concentration of 10.0 mg L^{-1} can be degraded over N-C/Co@PSS + PMS system within 15 min for 30 runs' operation. In addition, detailed non-radical dominating degradation mechanism was explored by active species capture experiments, electron spin resonance (ESR) tests and electrochemical technology. Furthermore, continuous degradation of TCs antibiotics for up to 200 h in the packed N-C/Co@PSS fixed bed reactors could be accomplished. This work provides theoretical and technical support for the application of MOFs-based catalysts in large-scale wastewater remediation.

1. Introduction

In recent years, many approaches including adsorption [1,2], membranes separation technology [3] and advanced oxidation process (AOPs) [4] have been explored for water decontamination. Among all treatment technologies, persulfate advanced oxidation processes (PS-AOPs) via activation of peroxodisulfate ($S_2O_8^{2-}$, PDS) or peroxymonosulfate (HSO_5^-, PMS) have received increasing attention [5]. Up to date, the degradation mechanisms of PS-AOPs could be summarized into the free radical pathway [6] and nonradical pathway [7]. Typically, the free radical pathway dominated by sulfate radical ($SO_4^{\bullet}$) has the advantages of (i) higher redox potential (2.5–3.1 V); (ii) longer half-life (30–40 μs) and (iii) wider suitable range of pH (2.0–9.0) [5]. On the other part, three primary nonradical pathways like electron-transfer processes [8], singlet oxygenation [9] and high-valent metal induced oxidation [10] have been widely explored and reported. Nonradical oxidation exhibited the merits of resistance to environmental influences, selection for substances and adjustable redox potential [11]. However, the current popular catalysts with the form of particles or powder were almost limited in recyclability and reusability [12]. Therefore, the development of new composition and specially immobilized catalyst with high activity and facile recovery for persulfate activation are important, yet challenging.

In view of the above, many attempts have been made to granulate and extrude catalysts into large size materials or to synthesize them into monoliths to overcome the shortcomings of difficult recovery from aqueous solutions [13,14]. However, these processes involved complicated treatments and instrumentations. On the other hand, the active site and surface area of the catalysts obtained by these methods are limited due to the encapsulation of nanoparticles by the additives layer.

* Corresponding author at: Beijing Key Laboratory of Functional Materials for Building Structure and Environment Remediation, Beijing University of Civil Engineering and Architecture, Beijing, 100044, China.
E-mail address: wangchongchen@bucea.edu.cn (C.-C. Wang).

https://doi.org/10.1016/j.cej.2022.138082
Received 17 May 2022; Received in revised form 3 July 2022; Accepted 11 July 2022
Available online 19 July 2022

To this end, there is an urgent need for a catalyst that can be used for in-situ immobilization.

Metal-organic frameworks (MOFs) are typically synthesized via the coordination bonding interactions between metal ions and organic linkers [15], displaying the characteristics of huge specific surface area, abundant nanopores and the ability to be immobilized easily on the surface of large particle materials [16]. Especially, Co-based MOFs, represented by ZIF-67 [17], have been used as effective non-homogeneous catalysts for activation of PMS/PDS because of their abundance of divalent Co species [18], which exhibit excellent PMS/PDS activation efficiency attributed to the particular 3d band structure of Co^{2+} [19]. To date, ZIF-67 has been immobilized on numerous substrates, such as electrospun polyacrylonitrile [20], ion exchange resins [21] and nickel foam [22] to activate PMS/PDS for the removal of organic pollutants. The appropriate large-scale supports should be robust, industrially obtainable, chemically stable, affordable and surface-functionalized easily to realize in-suit growth. There is also a big challenge to enhance the catalytic properties.

Given these prerequisites, we propose to use commercially porous spherical substrate (PSS) as a macroscopic support for the growth of nanoscale ZIF-67. PSS is a siliceous material which is originally used in aquarium filter media with the properties of robustness, inexpensiveness, large surface area and resistance to high temperature, allowing it to be used in a wide range of liquid-based processes [23]. The inherent surface features of PSS and ZIF-67 make them easy to bind with each other. The high-temperature resistance also allows for further derivatization of ZIF-67 to prepare some derivatives like Co_3O_4 [24] and cobalt/carbon nanocomposites [25] with higher catalytic activity and stability.

Herein, a new immobilized heterogeneous catalyst N—C/Co@PSS derived from ZIF-67@PSS was developed to accomplish the activation of PMS for efficient TCs mixture of tetracycline (TTC), oxytetracycline (OTC) and chlortetracycline (CTC) degradation (the chemical information of the above-mentioned TCs can be found in the **Table S1**). TCs removal efficiency in this PS-AOP system was investigated. In addition, scavenger quenching experiments, electron spin resonance (ESR) technology and electrochemical techniques were used to explore the mechanisms. Last but not the least, separation-free use of N—C/Co@PSS catalysts and flow-through purification of antibiotic-containing wastewater were achieved over the continuous operation units.

2. Experimental

2.1. Materials and characterizations

All information of the chemicals and reagents (**Text S1**), characterization instruments and methods (**Text S2**) are provided in the Supplementary Information (SI).

2.2. Preparation of immobilized catalysts

The synthesis procedure includes two steps as shown in **Fig. S1**.

(i) The synthesis of ZIF-67/PSS precursor: $Co(NO_3)_2{\cdot}6H_2O$(2.0814 g) and 2-methylimidazole(5.7468 g) were dissolved in 150.0 mL of methanol, respectively. After sufficient dissolution, four commercial porous spherical substrates (PSSs) with a diameter of 20.0 mm were immersed in the $Co(NO_3)_2$ methanol solution for 20.0 min. After that, these four PSSs were transferred to the methanol solution of 2-methylimidazole and immersed for another 20.0 min. The above-mentioned immersion steps were repeated three times. Finally, the treated PSSs were immersed in the mixture of $Co(NO_3)_2$ and 2-methylimidazole methanol solution for 12 h at the room temperature. The as-obtained purple immobilized material was washed with methanol for three times, and dried in at 333 K for 10 h to obtain ZIF-67/PSS precursors.

(ii) The synthesis of N—C/Co@PSS: The prepared ZIF-67/PSS was pyrolyzed in N_2 atmosphere under the temperature of 500 °C for 3.0 h to obtain the immobilized catalysts N—C/Co@PSS, which was dried at 333 K for 24 h after being washed by ethanol and deionized water. It was calculated that the average N—C/Co load onto each PSS was 20.0 mg.

2.3. Catalytic PMS activation for TCs degradation over N—C/Co@PSS in batch experiments

During the batch-type experiments, all reactions were conducted under dark conditions, in which the catalytic properties of N—C/Co@PSS was assessed by degrading TCs matrix including OTC, TTC and CTC at an initial concentration of 10.0 mg L^{-1}, respectively. The H_2SO_4 or NaOH solutions with suitable concentrations were adopted to adjust the solution pH in the range from 3.0 to 10.0. A piece of N—C/Co@PSS immobilized catalyst (effective catalyst dosage being 400.0 mg L^{-1}) and 0.15 mM PMS were introduced to the reactor, in which the TCs degradation experiments were initiated by continuous stirring at 200.0 rpm at room temperature. 1.5 mL solution was filtrated from the reactor at predetermined time intervals using a syringe with 0.22 μm PTFE filters to determine the residual TCs concentrations, which was quenched immediately with excess methanol for further determination. The high-performance liquid chromatograph (HPLC, Vanquish Duo) equipped with a C18 column (2.1 mm × 250 mm, 5.0 μm) was used to determine the residual concentrations of TCs, in which the detection wavelength of the UV detector was fixed at 355 nm.

2.4. Catalytic PMS activation for continuous TCs degradation over N—C/Co@PSS immobilized catalysts in the fixed-bed reactor

As depicted in Scheme. 1**a, 15** pieces of N—C/Co@PSS with approximately 300 mg of effective N—C/Co catalyst were packed into a columnar fixed-bed reactor with a reaction volume of 100.0 mL, in which a peristaltic pump and a high precision syringe pump were used to feed the targeted solution a flow rate of 10.0 mL min^{-1} and PMS solution a flow rate of 20.0 μL min^{-1}, respectively.

2.5. Modular-based coupling AOP processes for continuous TCs degradation in different fixed-bed reactors

As depicted in Scheme. 1**b, 15** pieces of N—C/Co@PSS with 300 mg effective N—C/Co catalyst and 10 pieces of N—C/Co@PSS with 200.0 mg effective N—C/Co catalyst were packed in the 100.0 mL column fixed-bed reactor (#1 and #2 reactor) and the 60.0 mL column fixed-bed reactor (#3 reactor), respectively. An ultraviolet (UV) lamp (5 W) was installed in reactor 3 without any catalyst. A peristaltic pump and a high-precision syringe pump were adopted to feed targeted solution and PMS solution to the #1 reactor. The #2 reactor was connected to receive the effluent from #1 reactor, in which an ozone generator was introduced to provide O_3 for accomplishing catalytic ozonation over N—C/Co@PSS. The #3 reactor received the effluent of #2 reactor, in which a high-precision syringe pump was used to feed PDS to achieve UV light-activated peroxydisulfate process (UV/PDS).

3. Results and discussion

3.1. Characterization of catalysts

The scanning electron microscopy (SEM) image shows that the pristine PSS substrate displayed laminate structure with smooth surface (Fig. 1**a**). The original PSS, as siliceous material, consisted mainly of Si, C and O (**Fig. S2**). By contrast, the modified PSS by ZIF-67 particles showed rough surface as the fine particles with the particle size of ca. 500 nm were coated on the surface of PSS (Fig. 1**b**) [26]. Transmission electron microscopy (TEM) image of as-obtained N—C/Co@PSS via pyrolysis at 500 °C under N_2 atmosphere (Fig. 1**c and 1d**) demonstrated that the wrinkled *ortho*-polyhedral particles with particle size of ca. 400 nm were adhered to the surface of PSS. The high-resolution TEM image (Fig. 1**e**) indicated that N—C/Co particles immobilized on PSS displayed

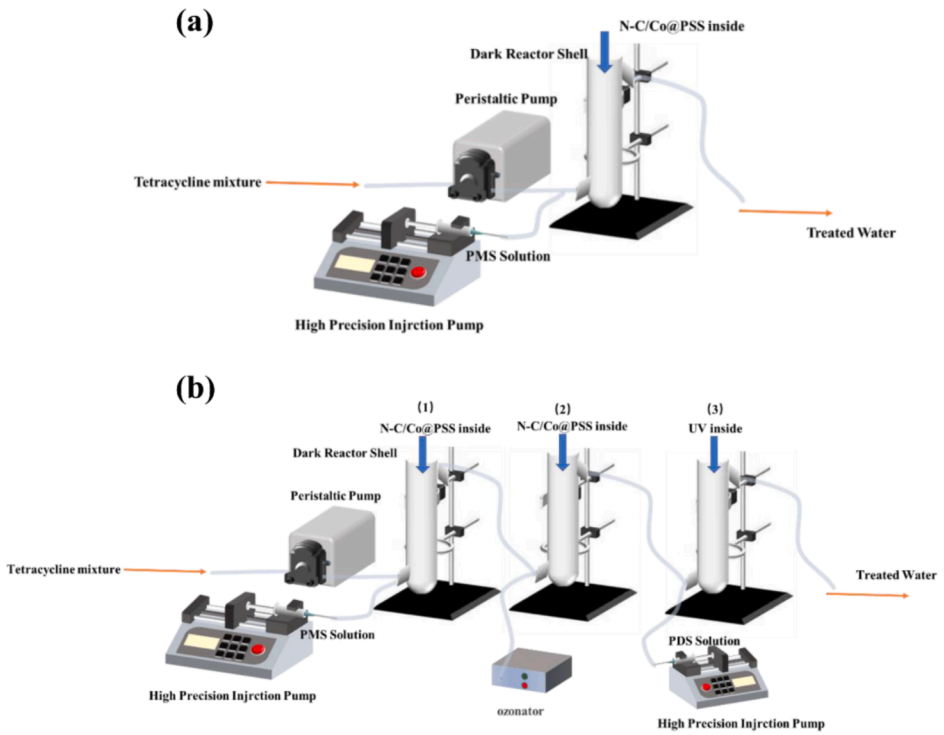

Scheme 1. Schematic diagram of (a) fixed-bed continuous flow reactor based on PS-AOPs and (b) the coupling fixed-bed continuous flow reactors (#1 reactor: PMS/N—C/Co@PSS; #2 reactor: O_3 /N—C/Co@PSS; #3 reactor: UV/PDS).

clear lattice diffraction fringes of Co^0 (orange dotted area) and graphite carbon (the blue dotted area), in which the lattice distances of 0.204 nm and 0.343 nm corresponded to the (1 1 1) crystalline facet of the Co^0 element [27] and the (0 0 2) fringe of graphite carbon [28], respectively. Besides, the EDS determination of N—C/Co@PSS (Fig. 1**f**) exhibited that the elements of C, Co and N with the mass ratio of 6.1:2.9:1 (**Table S2**) are uniformly dispersed on the surface of the catalyst, where the N derived from the 2-methylimidazole ligand was doped to the graphite carbon [29].

It was difficult to observe the characteristic X-ray diffraction (XRD) patterns of ZIF-67 and N—C/Co in the ZIF-67@PSS and N—C/Co@PSS (**Fig. S3a**), due to the relatively low-load amount. The XRD patterns of the ZIF-67 and N—C/Co powders synthesized under the identical conditions to the immobilized materials displayed the characteristic XRD peaks of ZIF-67 and N—C/Co (**Fig. S3b**), comparable to the reported patterns in the literature [30,31]. After pyrolysis, characteristic peaks of 2-theta 26° and 44.2° corresponded to the (0 0 2) crystal plane of graphitic carbon [32] and the (1 1 1) crystal plane of Co^0 [33], respectively, which coincided with the results of HRTEM. The presence of N—C/Co in PSS was further confirmed by X-ray photoelectron spectroscopy (XPS) (**Fig. S4**) and the corresponding results and discussions were discussed in SI (**Text S3**).

3.2. Catalytic PMS activation for TCs degradation in batch experiments

The OTC, TTC and CTC degradation efficiencies via PS-AOP over different catalysts were presented in Fig. 2**a**, Fig. 2**b** and Fig. 2**c**, respectively. The self- decomposition efficiency of PMS for OTC, TTC and CTC was up to 75.9 %, 63.5 % and 71.7 % within 15 min, which could be contributed to the generation of ROSs such as $SO_4^{\bullet}$ and $^1O_2$ from the PMS hydrolysis (Eqs. 1 and 2) [34]. Without the presence of PMS, the adsorption capacities of N—C/Co@PSS towards OTC, TTC and CTC were 31.5%, 19.2% and 37.3% within 15 min, respectively, which could concentrate the TCs to be attacked by the active species during PS-AOP reactions [35]. In the PSS + PMS system, the catalytic degradation performance was slightly enhanced compared to that of individual PMS due to the possible contribution of metal impurities in the PSS substrate (**Table S3**) to the PMS activation. In the presence of both N—C/Co@PSS catalyst and PMS, 100% removal efficiencies of OTC, TTC and CTC were achieved within 15 min, demonstrating that the immobilized N—C/Co@PSS catalyst could effectively activate PMS to yield ROSs to achieve efficient degradation toward different TCs. In addition, the PS-AOP degradation rates for TCs over N—C/Co@PSS was further evaluated using a pseudo-first-order kinetic model ($-\ln(C/C_0) = kt$)) [36]. The removal rate constants k of OTC, TTC and CTC in the N—C/Co@PSS + PMS system were 0.2687, 0.3519 and 0.2591 min^{-1}, respectively, which were much higher than those of the other control systems (Fig. 2**d,** Fig. 2**e and** Fig. 2**f**). The above results demonstrated that the N—C/Co@PSS was an excellent catalyst to activate PMS for accomplishing high degradation efficiency and superior degradation rate. To investigate the TCs degradation process, the TOC removal efficiency was explored. As illustrated in **Fig. S5**, the TOC removal efficiency increased as the reaction progressed, and 28.2% of TOC could be removed over N—C/Co@PBS + PMS system within 60 min, indicating that TCs can be partially mineralized to CO_2 and H_2O. The produced ROSs and the corresponding degradation mechanisms are discussed in the subsequent sections.

$$HSO_5^- \rightarrow SO_4^{\bullet} + \bullet OH \quad (1)$$

$$SO_5^{2-} + HSO_5^- \rightarrow HSO_4^- + SO_4^{2-} + {}^1O_2 \quad (2)$$

3.3. The influences of operational parameters, universality and reusability

The effect of initial pH on TCs degradation over N—C/Co@PSS + PMS system was depicted in **Fig. S7**. The results revealed that N—C/Co@PSS could effectively activate PMS for TCs degradation in a wide pH operating window (3.0–9.0). The degradation efficiency was enhanced as the pH increased, which could be attributed to the various speciation of PMS at variable pH conditions [37].

Some general anions such as Cl^-, NO_3^- and $H_2PO_4^-$ in the aqueous

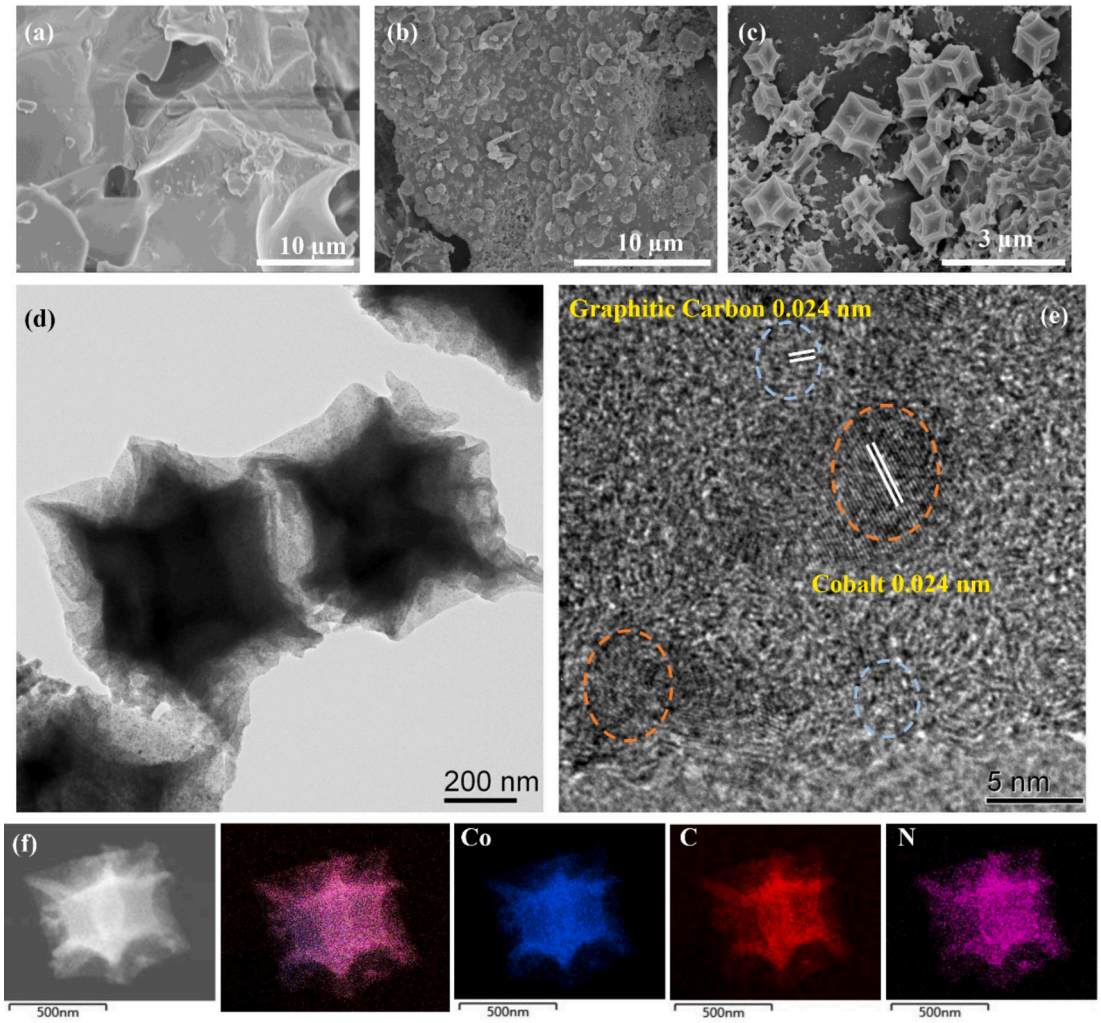

Fig. 1. The SEM images of (a) PSS, (b) ZIF-67/PBS and (c) N—C/Co@PSS; (d and e) The HRTEM images of N—C/Co@PSS; (f) The EDS elemental mapping images of N—C/Co@PSS.

environment may adversely affect the reaction efficiency of PS-AOPs [38]. The effects of inorganic anions on the removal of TCs were studied based on the concentrations of inorganic anions in Beijing surface water [39]. The experimental results showed that the three above-mentioned anions exhibited slight inhibition effect on the TCs degradation (Fig. S9), due to that the inorganic anions like Cl^-, NO_3^- and $H_2PO_4^-$ could serve as quenchers of free radicals in AOPs or $SO_4^{\bullet}$ could react with inorganic anions to generate free radicals of weakly oxidation performance [40]. However, the degradation efficiency of the three tetracycline antibiotics still reached to ca. 100% within 15 min even in the presence of different inorganic anions, demonstrating that the N—C/Co@PSS + PMS system was highly adaptable to the environment. It was also suggested that non-radical degradation pathways may exist in this catalytic system. The TCs removal efficiencies over N—C/Co@PSS + PMS system in different water matrixes were also evaluated, in which tap water and lake water were adopted to formulate the simulated polluted water containing different TCs (Table S4). As shown in Fig. S10**a**, the OTC degradation efficiencies could reach 95.9% and 96.8% in tap water and lake water, and the degradation performances toward TTC (Fig. S10**b**) and CTC (Fig. S10**c**) were also not inhibited. The excellent removal performance in real water matrix indicated that the immobilized N—C/Co@PSS catalyst processes the potential to treat antibiotic wastewater in practical situations.

3.4. The universality and reusability

To further evaluate the application prospects of the N—C/Co@PSS + PMS system, the degradation performances of N—C/Co@PSS toward organic pollutants such as sulfamethoxazole (SMX), bisphenol-A (BPA), atrazine (ATZ) and 2,4-dichlorophenoxyacetic acid (2,4-D) with the initial concentration of 10.0 mg L^{-1} were investigated under the optimal reaction conditions. Within 15 min, the SMX, BPA, ATZ and 2,4-D removal efficiencies could also reach 100%, 100%, 91.5% and 95.9% (Fig. S8), respectively, suggesting the excellent catalytic property of N—C/Co@PSS for PMS activation towards various organic pollutants.

The recyclability of catalysts is an important element to evaluate the catalysis properties [41]. As shown in Fig. 3**a**, the catalytic degradation efficiencies of N—C/Co@PSS toward OTC, TTC and CTC could still reach 95.9%, 97.9% and 93.9% within 30 runs' operation, which exhibited superior catalytic activity on TCs degradation to the bench counterpart catalysts (Table S5). The leached Co ions decreased significantly during the operation, in which 0.20 mg L^{-1} of leached cobalt ion was detected in the 30th cycle (Fig. S11), far below the specified value (1 mg L^{-1}) in *Emission standard of pollutants for copper, nickel, cobalt industry*" (GB 25467–2010). By comparing the SEM images of N—C/Co@PSS before and after the PS-AOP reaction, it was found that the original morphology and loading of N—C/Co@PSS could still be successfully maintained after 30 runs (Fig. 3**b**), further demonstrating the excellent stability and reusability of the as-prepared N—C/Co@PSS.

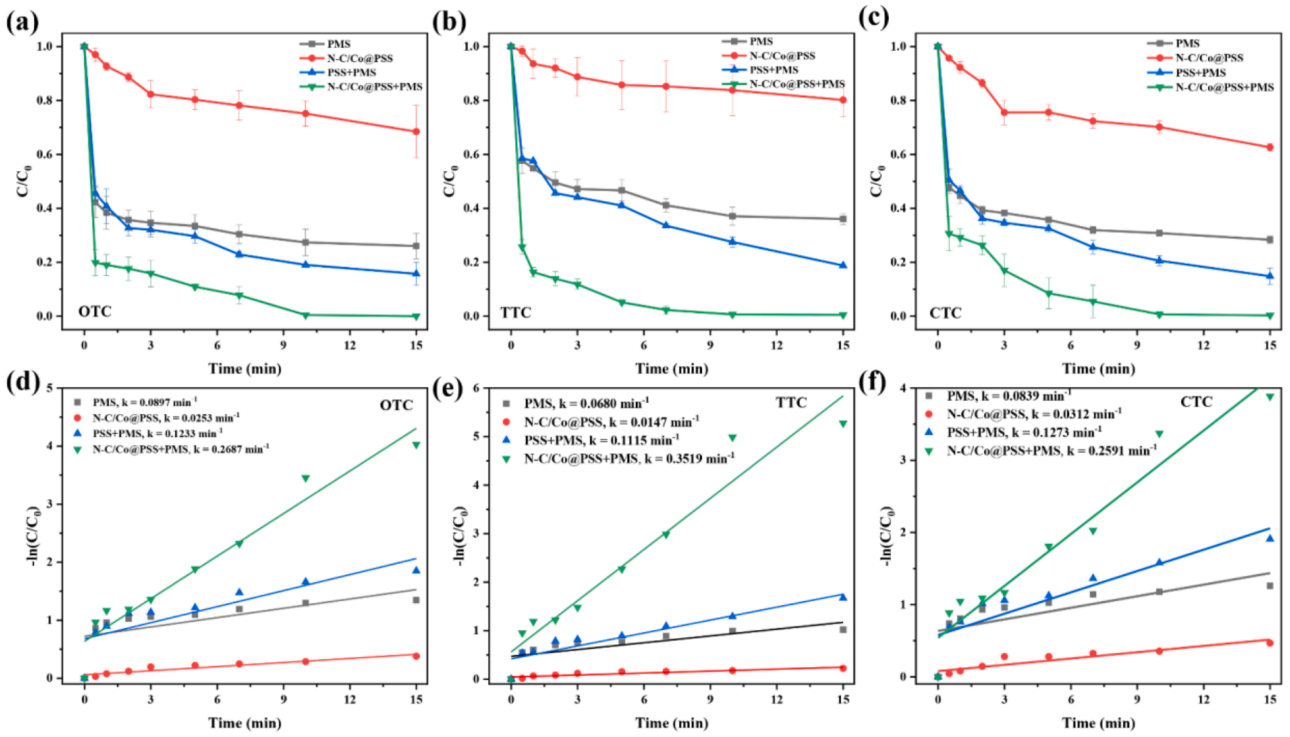

Fig. 2. The degradation efficiency of TCs (a: OTC; b: TTC and c: CTC) over N—C/Co@PSS + PMS system; The corresponding *k* value (e: OTC; f: TTC and g: CTC) of tetracycline antibiotics degradation over N-C/Co@PSS + PMS system. Conditions: Catalyst = 400.0 mg L^{-1}, OTC = 10.0 mg L^{-1}, TTC = 10.0 mg L^{-1}, CTC = 10.0 mg L^{-1}, PMS = 0.15 mM, pH = 4.3.

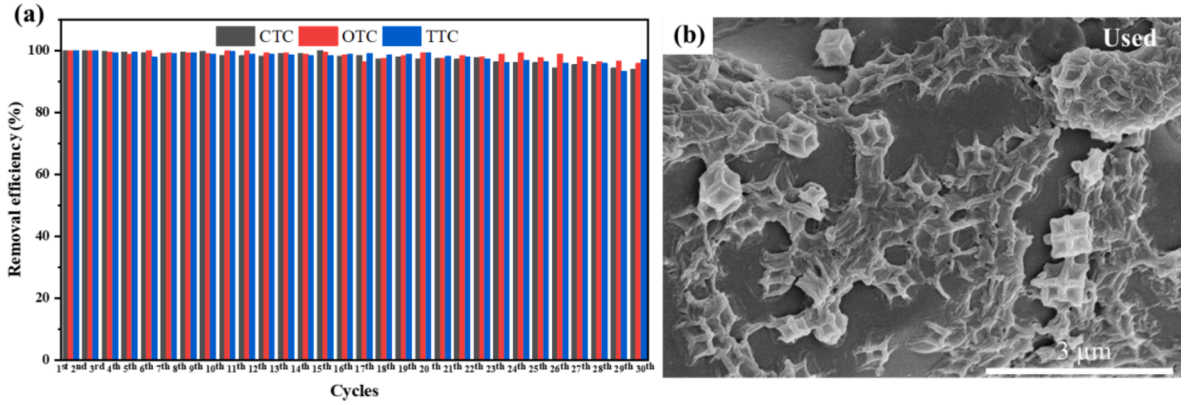

Fig. 3. (a) Removal efficiencies of TCs over N—C/Co@PBS + PMS system in 30 consecutive runs Conditions: Catalyst = 400.0 mg L^{-1}, OTC = 10.0 mg L^{-1}, TTC = 10.0 mg L^{-1}, CTC = 10.0 mg L^{-1}, PMS = 0.15 mM, pH = 4.3. The SEM images of N—C/Co@PBS after (b) 30 cycles reaction of batch experiment.

3.5. The possible mechanisms of PMS activation over N—C/Co@PBS for TCs degradation

Typically, there are two main degradation pathways for the activation of PMS: free radical degradation and non-free radical degradation [42]. To identify the main ROSs in the N—C/Co@PBS + PMS system for TCs degradation, the scavenger quenching experiments were conducted. Methanol (MeOH, 150 mM, $k_{SO_4^{\bullet-}}$ = 1.2–2.8 × 10^9 M^{-1} s^{-1}) [43], *tert*-butanol (TBA, 150 mM, $k_{\bullet OH}$ = 3.8–7.6 × 10^8 M^{-1} s^{-1}) [44], benzoquinone (BQ, 150 mM, $k_{\bullet O_2^-}$ = 0.9–1.0 × 10^9 M^{-1} s^{-1}) [45], and L-histidine (75 mM, 150 mM, k^1O_2 = 3.2 × 10^7 M^{-1} s^{-1}) [46] were used as the capture agents of $SO_4^{\bullet-}$, •OH, $\bullet O_2^-$ and $^1O_2$, respectively. The OTC degradation efficiencies were inhibited by 13.3%, 3.7% and 8.7% when MeOH, TBA and BQ were added to the solution, respectively (Fig. 4**a**). The final once L-histidine with concentration of 75 mM was introduced, the OTC degradation efficiency declined from 100% (no scavenger) to 74.1%. When the concentration of L-histidine was increased from 75 mM to 150 mM, the OTC removal efficiency further declined from 74.1% to 61.3%, indicating that $^1O_2$ might be the dominant reactive specie for OTC degradation in this system. Similarly, the magnitude of the role played by the active substances in the degradation toward TTC and OTC followed the order of $^1O_2$ > $SO_4^{\bullet-}$ > •OH > $\bullet O_2^-$ (Fig. 4**b** and Fig. 4**c**).

Electron spin resonance (ESR) technology was further performed to examine the generation of the different ROSs with the coexistence of 2,2,6,6-Tetramethylpiperidone (TEMP) and 5,5-dimethyl-1-pyrroline (DMPO), It could be observed in Fig. 4**d** that the obvious 1: 1: 1 triplet-peak signal of $^1O_2$ were detected in N-—C/Co@PSS + PMS system [47], and the intensity of signals became stronger as time progressed (Fig. 4**d**), indicating the continuous generation of $^1O_2$. As shown in Fig. 4**e**, The signals of DMPO-$SO_4^{\bullet-}$, DMPO-•OH and DMPO-$\bullet O_2^-$ were observed in N—C/Co@PSS + PMS system [48,49], implying the presence of $SO_4^{\bullet-}$, •OH and $\bullet O_2^-$. Based on the ESR results, both $^1O_2$, $SO_4^{\bullet-}$, •OH

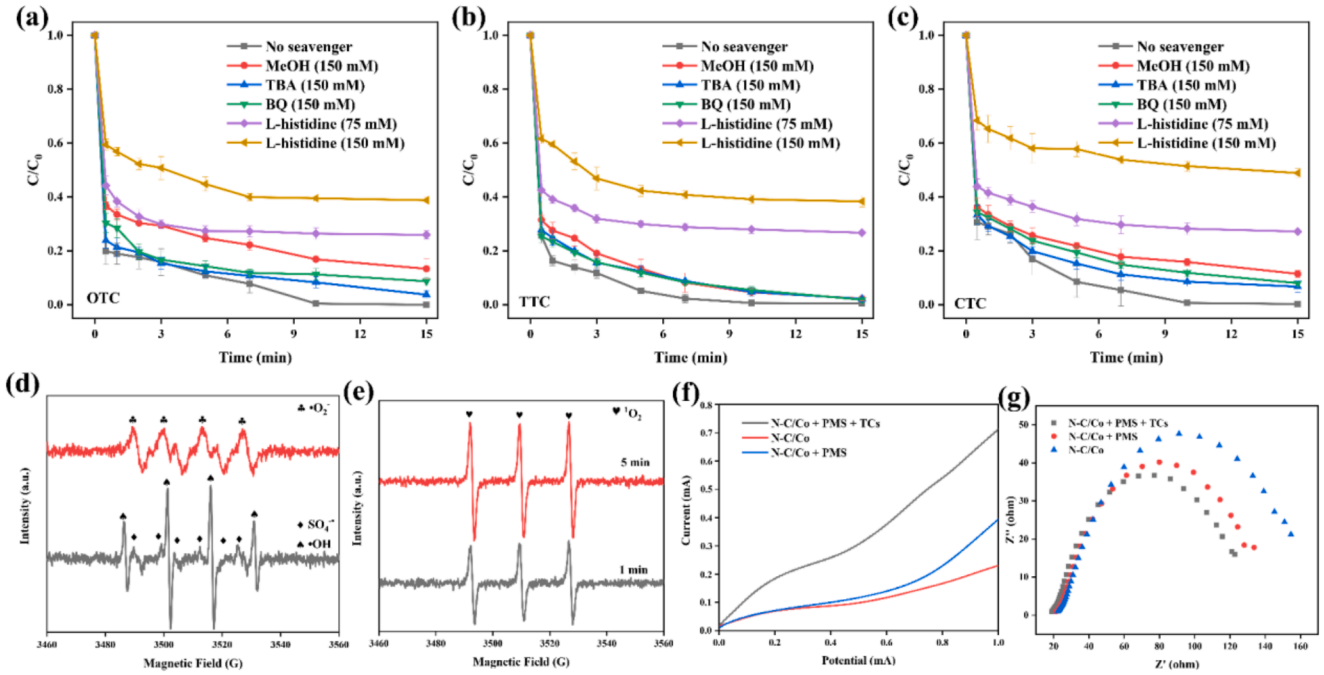

Fig. 4. Influences of different capturers on TCs (a: OTC; b: TTC and c: CTC) degradation efficiencies over N-C/Co@PBS + PMS system. Conditions: Catalyst = 400.0 mg L^{-1}, OTC = 10.0 mg L^{-1}, TTC = 10.0 mg L^{-1}, CTC = 10.0 mg L^{-1}, PMS = 0.15 mM, pH = 4.3. (d) TEMP-$^1O_2$, (e) DMPO-$SO_4^{\bullet}$, DMPO-•OH and DMPO-$\bullet O_2^-$ in the N—C/Co@PBS + PMS system. (f) Linear sweep voltammetry curves and (g) Electrochemical impedance spectroscopy analysis obtained under different conditions.

and $\bullet O_2^-$ were generated during the PS-AOPs reaction, which were consistent with the quenching experiments.

In recent years, as the typically non-radical oxidation mechanism, electron transfer processes have been widely reported for the degradation of organic pollutants [8]. In this work, electrochemical techniques were performed to identify the electron transfer processes in the N—C/Co@PBS + PMS system. Due to the relatively minor loading, it was difficult to test N—C/Co@PBS directly, and the N—C/Co powder material was selected for electrochemical testing. The linear sweep voltammetry (LSV) results (Fig. 4**f**) showed that the current density enhanced notably with the addition of PMS, indicating that PMS interacted with N—C/Co catalyst to form the metastable reactive complex. The current increased significantly after adding TCs, which suggested the TCs degradation had occurred and the formation of an electric flow formed from TCs to N—C/Co + PMS complex [50]. Electrochemical impedance spectroscopy (EIS) tests were carried out to estimate the conductivity of the catalyst. As shown in Fig. 4**g**, the semicircle size of N—C/Co + PMS + TCs decreased significantly compared to N—C/Co + PMS and N—C/Co alone, demonstrating the faster electron transfer rate in the presence of both catalysts, PMS and TCs [51]. In summary, in the N—C/Co@PBS + PMS + TCs system, electrons were transferred from TCs to PMS over N—C/Co, which could be contributed to TCs decomposition.

To further investigate the contributions of Co, C and N in the PS-AOPs reaction, XPS spectra of fresh and used N—C/Co@PBS were studied. For the fresh catalyst, the XPS spectrum of Co 2p (Fig. 5**a**) revealed the presence of Co^0 (780.3 eV) and Co^{2+} (781.8 eV) [52,53]. However, after the reaction, 27.0 % of Co^{3+} (782.4 eV) was produced with the percentage of Co^0 decreasing from 43.6 % to 35.9 %, suggesting that the reaction between Co^0 and PMS resulted in the oxidation of Co^0 to Co^{2+} and even Co^{3+} as well as the production of $SO_4^{\bullet}$ (**Eq. 3 and Eq. 4**) [26]. In addition, Co^{3+} could be reduced to Co^{2+} in turn via the reaction with HSO_5^- (**Eq. 5**) [54]. In the C 1 s spectra (Fig. 5**b**), four peaks centered at 284.2, 285.0, 285.9 and 287.5 eV can be indexed to C—C, C-OH, C—N and C—O bonds, respectively [55]. After the reaction, the C-OH bond disappeared, and both the relative proportions and positions of the C—C, C—O and C—N bonds had been changed, indicating the engagement of element C in the reaction. According to previous studies, electrons at the zigzag edges of carbon were highly chemically active to activate PMS to generate $SO_4^{\bullet}$ (**Eq. 6**) or $^1O_2$ [56]. The N 1 s spectra (Fig. 5**c**) displayed three peaks corresponding to pyridinic N (398.3 eV), pyrrolic N (399.0 eV) and graphite N (400.5 eV) [26], respectively. It has been reported that pyrrolic N in B and N co-doped CNT catalysts processed the ability for the acceleration of electron transfer and the activation of PMS [57]. In this study, the proportion of pyrrolic N decreased from 38.9 % to 30.7 % after the reaction, demonstrating that pyrrolic N was also the main active component in the activation of PMS.

$$Co^0 + 2HSO_5^- \rightarrow 2SO_4^{\bullet} + 2OH^- + Co^{2+} \quad (3)$$

$$Co^{2+} + HSO_5^- \rightarrow SO_4^{\bullet} + OH^- + Co^{3+} \quad (4)$$

$$Co^{3+} + HSO_5^- \rightarrow SO_5^{\bullet} + H^+ + Co^{2+} \quad (5)$$

$$e^- + HSO_5^- \rightarrow SO_4^{\bullet} + OH^- \quad (6)$$

To sum up, the mechanisms of the N—C/Co@PBS + PMS system for the degradation of TCs was depicted in Fig. 5**d**. (i) The Co element in the material can directly activate the PMS to produce $SO_4^{\bullet}$, which can further be converted in the system to •OH and $\bullet O_2^-$ and other radicals (**Eqs. 7–10**) [58] contributing to the degradation of TCs. (ii) The abundance of graphite C and pyrrolic N in N—C/Co@PBS not only directly activated PMS to produce active substances, but also accelerated the electron transfer during the PS-AOPs reaction as well as facilitated the reaction. (iii) The N—C/Co@PBS catalyst can be used as a transport mediator to enable the direct oxidation of TCs as electron donors through a mediated electron transfer process. (iv) $^1O_2$ generated via the activation of PMS by N—C/Co@PBS (Eq. 11), self-decomposition of PMS (**Eq. 2 and Eq. 12**) [26] and the conversion of $\bullet O_2^-$ (**Eq. 13**) [59] played a major role in the system for degradation of TCs. In conjunction with the PMS activation mechanisms of N—C/Co + PMS system, the possible degradation pathways of OTC, TTC and CTC were investigated according to the mass-to-charge ratio (*m/z*) of the intermediates measurement (**Fig. S12**, **Fig. S13** and **Fig. S14**, **the corresponding discussions** were clarified in **Text S4**, **Text S5** and **Text S6**).

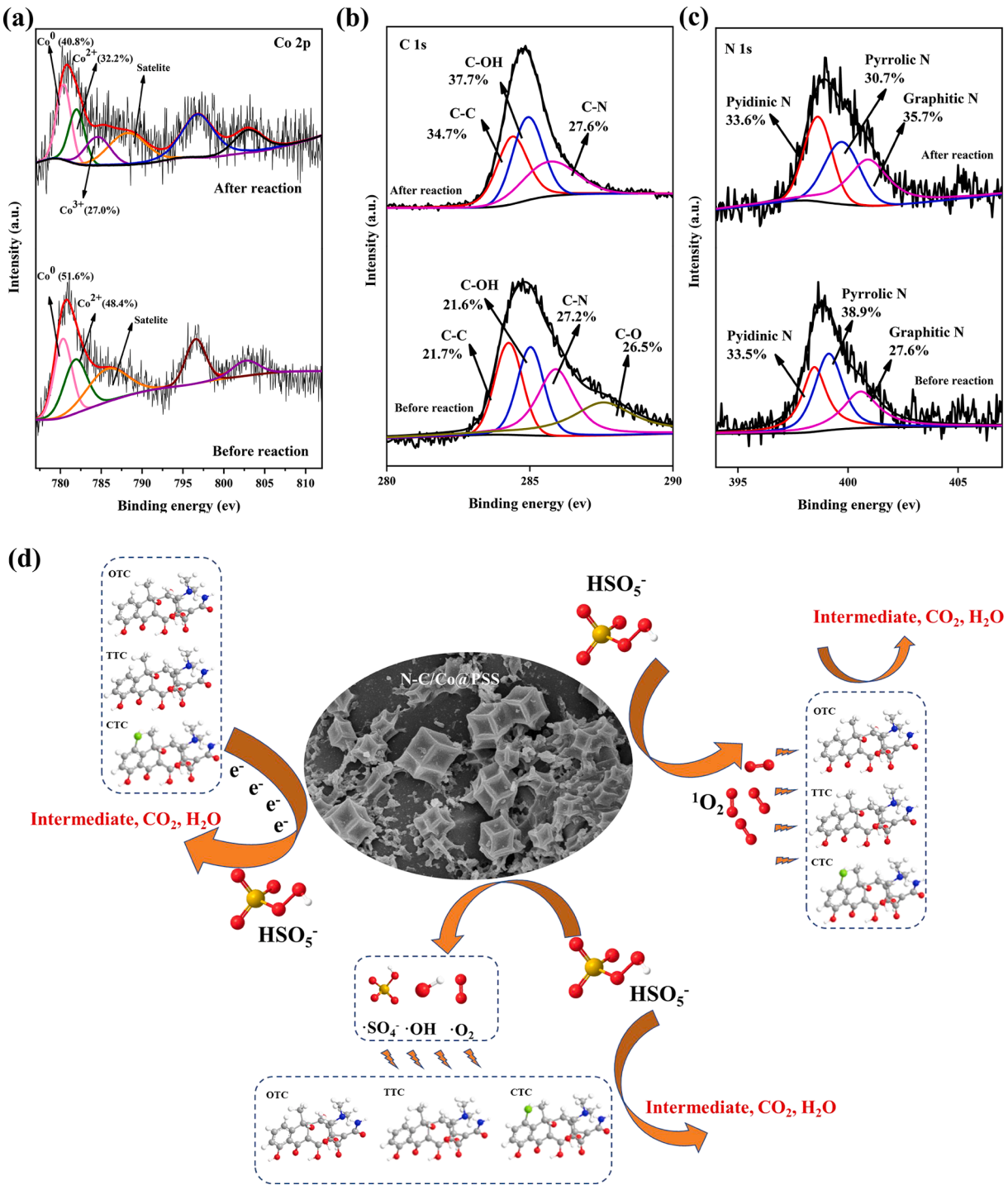

Fig. 5. (a) Co 2p, (b) C 1 s and (c) N 1 s XPS spectra of N—C/Co@PBS before and after the degradation reaction. (d) The possible mechanisms for TCs decomposition over N—C/Co@PBS + PMS system.

$$SO_4^{\bullet} + H_2O \rightarrow SO_4^{2-} + \bullet OH + H^+ \quad (7)$$

$$HSO_5^- + H_2O \rightarrow H_2O_2 + HSO_4^- \quad (8)$$

$$\bullet OH + H_2O_2 \rightarrow HO_2^{\bullet} + H2O \quad (9)$$

$$HO_2^{\bullet} \rightarrow H^+ + \bullet O_2^- \quad (10)$$

$$\text{N-C/Co@PBS}|2HSO_5^- \rightarrow \text{N-C/Co@PBS}|^1O_2 + 2H^+ + 2SO_4^{2-} \quad (11)$$

$$SO_5^{\bullet} + SO_5^{\bullet} \rightarrow {}^1O_2 + S_2O_8^{2-} \quad (12)$$

$$2O_2^{\bullet} + 2H_2O \rightarrow {}^1O_2 + H_2O_2 + 2OH^- \quad (13)$$

To investigate the changes in toxicity of the by-products during the degradation of TCs over N—C/Co@PSS + PMS system, the biological toxicity risk of the intermediates was assessed by quantitative structure–activity relationship (QSAR) based on Daphnia Magna LC_{50} [60]. As shown in Fig. S15, the acute toxicity of OTC and CTC was classified as toxic and TTC was harmful. Nevertheless, the LC_{50} values for most of the intermediates increased after the PS-AOPs reaction, indicating that the biotoxicity of OTC, TTC and CTC decreased during the degradation

process [60]. Therefore, N—C/Co@PSS + PMS system could not only completely degrade TCs but also reduce the biotoxicity of OTC, TTC and CTC, which was an efficient and green oxidation system.

3.6. Catalytic PMS activation for TCs degradation in continuous reaction system

According to the results of recyclable batch experiments, the prepared immobilized N—C/Co@PMS catalysts could effectively activate PMS for efficient TCs degradation with excellent recoverability and recyclability. Hence, we prepared a fixed-bed reactor (Fig. 6**a**) for continuous purification of simulated wastewater by N—C/Co@PSS + PMS, where the hydrodynamic residence time (HRT) was set as 10.0 min. As exhibited in Fig. S16, for 10.0 mg L^{-1} OTC, TTC and CTC, the continuous degradation efficiency of the only PMS did not exceed 50.0 % for the simulated wastewater. By contrast, TCs could be degraded efficiently over N—C/Co@PSS + PMS continuous system. Even after 200 h, the removal efficiency of OTC, TTC and CTC was still maintained at more than 97.4%, 96.8% and 85.1%, respectively (Fig. 6**b**). It was noteworthy to noting that the treatment of large-scale antibiotics could be achieved with only a small amount of PMS dosage (0.05 mM) compared to the PMS dosage in batch experiments (0.15 mM), reflecting the excellent catalytic performance of the immobilized catalyst in continuous purification. Similarly, for the OTC, TTC and CTC with low concentration of 1.0 mg L^{-1}, the ambition of long-term and efficient operation could also be achieved with relatively low cobalt ion leaching (Fig. S17). The corresponding discussions (**Text 6**) and experimental results (Fig. S18) were shown in SI. In addition, the SEM image (Fig. S19) of the used N—C/Co@PSS after the continuous process reflected its excellent long-term stability. Moreover, it could be calculated that 1.0 g N—C/Co catalyst in N—C/Co@PSS could accomplish purification treatment towards 400.0 L of wastewater containing antibiotics within 200 h. The above results mean that the greatly efficient utilization of catalysts and the reduction of catalyst costs will be achieved.

The operations in real water matrix are importantly to assess the performance and application prospects of the catalyst. To this end, mixed solutions containing OTC, TTC and CTC, each initial concentration of 10.0 mg L^{-1} were prepared with tap water and lake water (water quality parameters being listed in Table S4). As shown in Fig. S20, after 24 h of continuous operation, more than 95% removal efficiencies of TCs

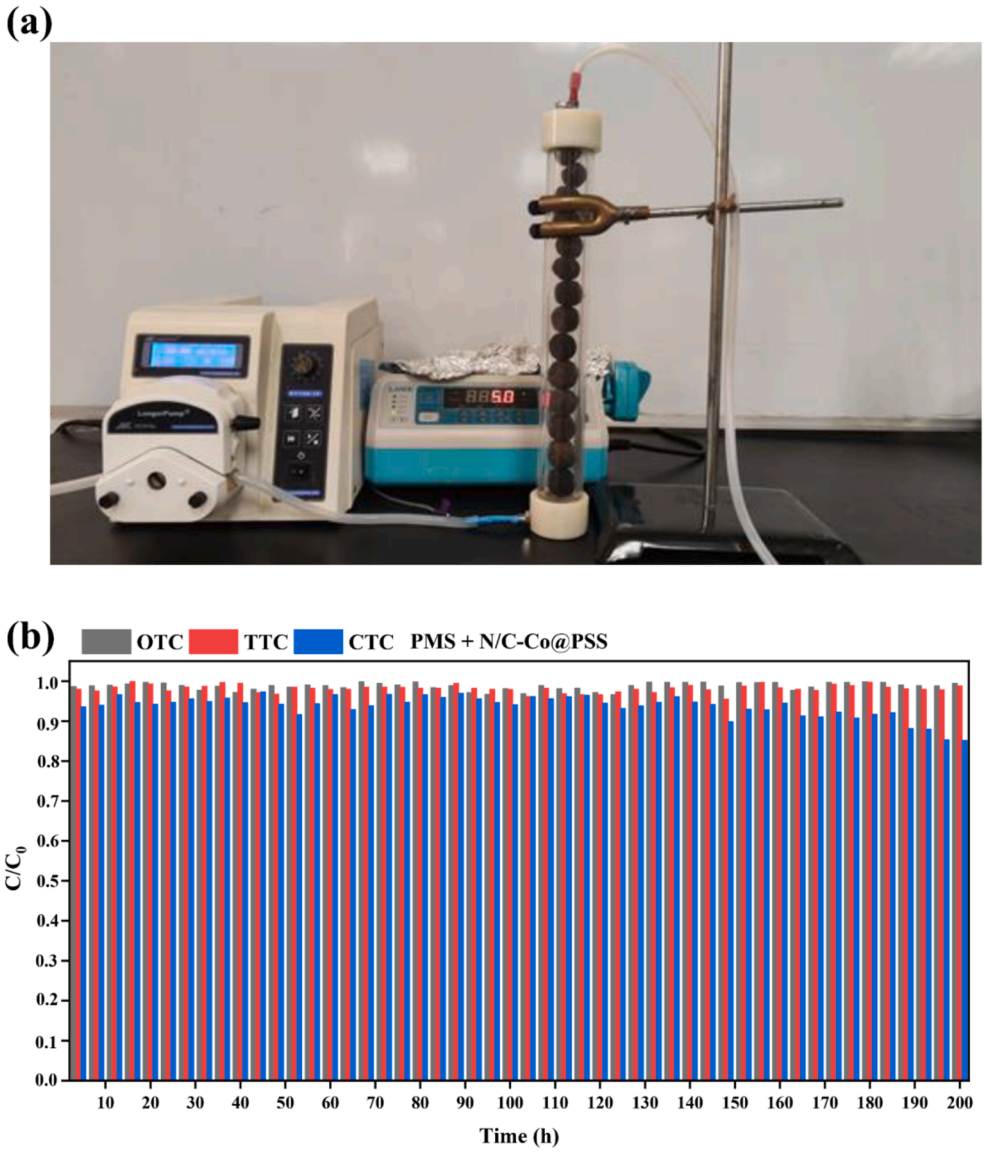

Fig. 6. (a) The photograph of fixed-bed continuous flow reactor based on PS-AOPs. (b) Continuous degradation of TCs over N—C/Co@PSS immobilization catalyst based on PS-AOPs. Conditions: Catalyst = 300 mg, $V_{PMS\ (250\ mM)}$ = 20 μL min^{-1}, OTC = 10.0 mg L^{-1}, TTC = 10.0 mg L^{-1}, CTC = 10.0 mg L^{-1}.

were achieved in simulated polluted water samples formulated with tap water and lake water, which was attributed to the non-radical-dominated degradation mechanism with low environmental impact in the water treatment process. The above-mentioned results demonstrated that the synthesized immobilized N—C/Co@PSS possessed promising potential for practical applications.

3.7. The continuous mineralization of TCs in modular-based coupling process of AOPs

When advanced oxidation processes are used for the end-of-pipe treatment of wastewater, it is essential to achieve zero discharge [61]. For this purpose, numerous coupling technologies based on AOPs have been developed [62]. In this research, triple AOPs technologies (N—C/Co@PSS + PMS, N—C/Co@PSS + O_3 and UV + PDS) had been modularly coupled (Fig. 7**a**). A series of controlled experiments (**Fig. S21**) were performed, and the detailed results were discussed in the SI (**Text S7**). In the modular continuous systems, the leached Co ions (0.86 mg L^{-1} after 72 h of treatment) along with the underutilized PMS and O_3 will all be further utilized in subsequent modules (**Eqs. 4, 14–18**) [63–66]. As shown in Fig. 7**b**, although the TOC removal efficiency in #1 reactor was only about 2%, the TOC removal efficiency could reach more than 20 % after passing through #2 reactor, which was mainly attributed to the transformation of large organic pollutants into small molecules and the efficient oxidation capacity of N—C/Co@PSS + O_3 [67]. Subsequently, the unmineralized by-products flowed into #3 reactor, where deep continuous mineralization with the TOC removal efficiency up to 70% was achieved by the synergistic activation of UV/PDS [68]. After 60 h of continuous operation, the TOC removal efficiency of #2 reactor decreased, which was speculated to the attribution of catalyst O_3 oxidation confirmed from the SEM image (**Fig. S22**). Affected by this, the TOC removal efficiency of #3 reactor also declined to 50%, approximately. Moreover, the growth inhibition tests of Escherichia coli (*E. coli*) were used to determine the toxicity of TCs and their intermediates during the AOPs coupling processes [69]. As shown in **Fig. S23**, three sets of parallel experiments were performed, in which the average diameters of inhibition zones for original TCs, #1 effluent, #2 effluent and #3 effluent against *E. coli*. were 17.0 mm, 10.8 mm, 10.0 mm and 8.8 mm, respectively. The above results indicated that the biotoxicity of the TCs decreased continuously over the modular AOPs coupling processes. The modular AOPs coupling process for the continuous system maximized the utilization of catalyst and achieved deep mineralization of the targeted pollutants in a continuous flow, providing technical support for the practical application of immobilized catalysts.

$$Co^{2+} + O_3 + H_2O \rightarrow Co(OH)^{2+} + \bullet OH + O_2 \quad (14)$$

$$SO_5^{\bullet-} + O_3 \rightarrow SO_4^{\bullet-} + 2O_2 \quad (15)$$

$$HSO_5^- + h\nu \rightarrow SO_4^{\bullet-} + \bullet OH \quad (16)$$

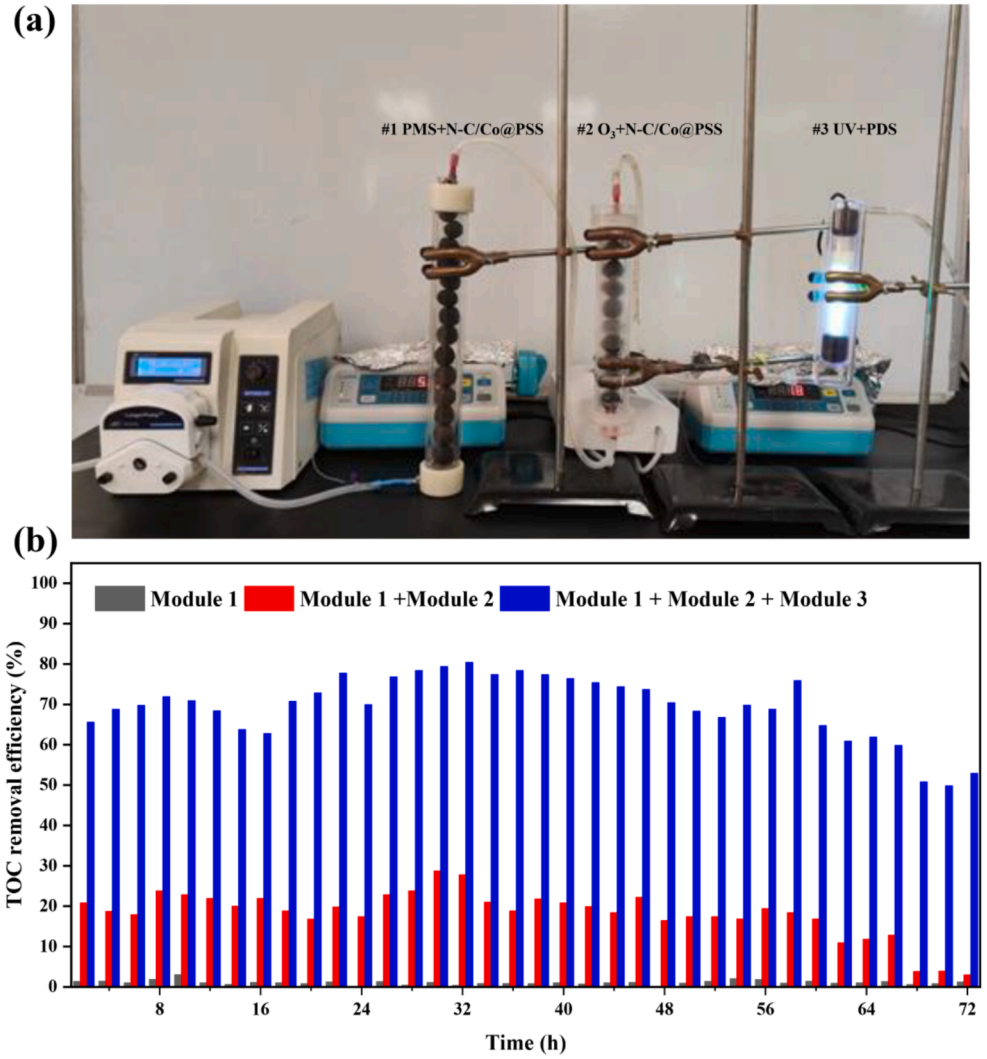

Fig. 7. (a) The coupling fixed-bed continuous flow reactors (#1 reactor: PMS/N—C/Co@PSS; #2 reactor: O_3/N—C/Co@PSS; #3 reactor: UV/PDS). (b) The TOC removal efficiency for continuous flow degradation of TCs over #1 reactor (PMS + N—C/Co@PSS system), #1 reactor (PMS + N—C/Co@PSS system) + #2 reactor (O_3 + N—C/Co@PSS system) and #1 reactor (PMS + N—C/Co@PSS system) + #2 reactor (O_3 + N—C/Co@PSS system) + #3 reactor (UV + PDS system). Conditions: OTC = 10.0 mg L^{-1}, TTC = 10.0 mg L^{-1}, CTC = 10.0 mg L^{-1}.

$$O_3 + h\nu \rightarrow \bullet O + O_2 \quad (17)$$

$$\bullet O + H_2O \rightarrow 2\bullet OH \quad (18)$$

4. Conclusion

In summary, N—C/Co@PSS (PSS, porous spherical substrate) immobilized catalyst derived from ZIF-67 was successfully prepared by pyrolysis, which could be confirmed by SEM, TEM, PXRD and XPS. In batch-type degradation, tetracycline antibiotics (TCs) matrix, containing oxytetracycline (OTC), tetracycline (TTC) and chlortetracycline (CTC) could be efficiently degraded via N—C/Co@PSS + PMS system within 15 min. The degradation mechanism was investigated via scavenger quenching experiments, electron spin resonance (ESR) tests, electrochemical and XPS analysis, revealing that no-radical ($^1O_2$) was the primary active specie, while other radicals ($SO_4^{\bullet}$, •OH and $\bullet O_2^-$) electron transfer process acted synergistically on the degradation of TC. N—C/Co@PSS possessed excellent stability and reusability confirmed from 30 cycles' consecutive batch-type experiments. In addition, the influences of operational parameters including PMS dosage, pH values, co-existing ions and real water matrix toward the removal performance of N—C/Co@PSS were discussed. Moreover, continuous treatment of wastewater was realized using a self-developed fixed reactor, and 1.0 g effective catalyst could achieve the purification of 400 L wastewater containing antibiotics within 200 h. Furthermore, through a modular-based coupling process (N—C/Co@PSS + PMS, ozonation, UV + PDS), continuous mineralization could be achieved effectively. This work demonstrated the enormous potential immobilized catalyst derived from MOFs for water remediation.

Declaration of Competing Interest

The authors declare that they have no known competing financial interests or personal relationships that could have appeared to influence the work reported in this paper.

Data availability

Data will be made available on request.

Acknowledgements

This work was supported by National Natural Science Foundation of China (51878023, 21806008), Beijing Natural Science Foundation (8202016), Great Wall Scholars Training Program Project of Beijing Municipality Universities (CIT&TCD20180323), Beijing Talent Project (2020A27), Science and Technology General Project of Beijing Municipal Education Commission (KM202110016010) and The Fundamental Research Funds for Beijing University of Civil Engineering and Architecture (X20147/X20141/X20135/X20146).

Appendix A. Supplementary data

Supplementary data to this article can be found online at https://doi.org/10.1016/j.cej.2022.138082.

References

[1] X. Ren, C.-C. Wang, Y. Li, C.-Y. Wang, P. Wang, S. Gao, Ag(I) removal and recovery from wastewater adopting NH_2-MIL-125 as efficient adsorbent: A 3Rs (reduce, recycle and reuse) approach and practice, Chem. Eng. J. 136306 (2022), 136306.
[2] C.-Y. Wang, L. Ma, C.-C. Wang, P. Wang, L. Gutierrez, W. Zheng, Light-response adsorption and desorption behaviors of metal–organic frameworks, Environ. Function. Mater. 1 (1) (2022) 49–66.
[3] X. Wang, Q. Lyu, T. Tong, K. Sun, L.-C. Lin, C.Y. Tang, F. Yang, M.D. Guiver, X. Quan, Y. Dong, Robust ultrathin nanoporous MOF membrane with intra-crystalline defects for fast water transport, Nat. Commun. 13 (2022) 266.
[4] X.-H. Yi, C.-C. Wang, Elimination of emerging organic contaminants in wastewater by advanced oxidation process over iron-based MOFs and their composites, Prog. Chem. 33 (2021) 471.
[5] X.-H. Yi, H. Ji, C.-C. Wang, Y. Li, Y.-H. Li, C. Zhao, A.o. Wang, H. Fu, P. Wang, X. u. Zhao, W. Liu, Photocatalysis-activated SR-AOP over PDINH/MIL-88A(Fe) composites for boosted chloroquine phosphate degradation: Performance, mechanism, pathway and DFT calculations, Appl. Catal. B Environ. 293 (2021), 120229.
[6] C. Zhao, J. Wang, X. Chen, Z. Wang, H. Ji, L. Chen, W. Liu, C.-C. Wang, Bifunctional $Bi_{12}O_{17}Cl_2$/MIL-100(Fe) composites toward photocatalytic Cr(VI) sequestration and activation of persulfate for bisphenol A degradation, Sci. Total Environ. 752 (2021), 141901.
[7] W. Peng, Y. Dong, Y. Fu, L. Wang, Q. Li, Y. Liu, Q. Fan, Z. Wang, Non-radical reactions in persulfate-based homogeneous degradation processes: A review, Chem. Eng. J. 421 (2021), 127818.
[8] W. Ren, C. Cheng, P. Shao, X. Luo, H. Zhang, S. Wang, X. Duan, Origins of Electron-Transfer Regime in Persulfate-Based Nonradical Oxidation Processes, Environ. Sci. Technol. 56 (2022) 78–97.
[9] E.-T. Yun, J.H. Lee, J. Kim, H.-D. Park, J. Lee, Identifying the Nonradical Mechanism in the Peroxymonosulfate Activation Process: Singlet Oxygenation Versus Mediated Electron Transfer, Environ. Sci. Technol. 52 (2018) 7032–7042.
[10] L. Pan, W. Shi, T. Sen, L. Wang, J. Zhang, Visible light-driven selective organic degradation by $FeTiO_3$/persulfate system: the formation and effect of high valent Fe(IV), Appl. Catal. B Environ. 280 (2021), 119414.
[11] W. Ren, L. Xiong, G. Nie, H. Zhang, X. Duan, S. Wang, Insights into the electron-transfer regime of peroxydisulfate activation on carbon nanotubes: the role of oxygen functional groups, Environ. Sci. Technol. 54 (2) (2020) 1267–1275.
[12] A. Du, H. Fu, P. Wang, C. Zhao, C.-C. Wang, Enhanced catalytic peroxymonosulfate activation for sulfonamide antibiotics degradation over the supported CoS_x-CuS_x derived from ZIF-L(Co) immobilized on copper foam, J. Hazard. Mater. 426 (2022), 128134.
[13] R. Guo, B. Xi, C. Guo, X. Cheng, N. Lv, W. Liu, A.G.L. Borthwick, J. Xu, Persulfate-based advanced oxidation processes: The new hope brought by nanocatalyst immobilization, Environ. Function. Mater. 1 (2022) 67–91.
[14] P. Küsgens, A. Zgaverdea, H.G. Fritz, S. Siegle, S. Kaskel, Metal-organic frameworks in monolithic structures, J. Am. Ceram. Soc. 93 (2010) 2476–2479.
[15] C.-Y. Wang, C.-C. Wang, X.-W. Zhang, X.-Y. Ren, B. Yu, P. Wang, Z.-X. Zhao, H. Fu, A new Eu-MOF for ratiometrically fluorescent detection toward quinolone antibiotics and selective detection toward tetracycline antibiotics, Chin. Chem. Lett. 33 (2022) 1353–1357.
[16] C.-C. Wang, X.-H. Yi, P. Wang, Powerful combination of MOFs and C_3N_4 for enhanced photocatalytic performance, Appl. Catal. B Environ. 247 (2019) 24–48.
[17] X.-W. Zhang, M.-Y. Lan, F. Wang, X.-H. Yi, C.-C. Wang, ZIF-67-based catalysts in persulfate advanced oxidation processes (PS-AOPs) for water remediation, J. Environ. Chem. Eng. 10 (2022), 107997.
[18] C. Wang, P. Cheng, Y. Yao, Y. Yamauchi, X. Yan, J. Li, J. Na, In-situ fabrication of nanoarchitectured MOF filter for water purification, J. Hazard. Mater. 392 (2020), 122164.
[19] M. Puche, L. Liu, P. Concepción, I. Sorribes, A. Corma, Tuning the Catalytic Performance of Cobalt Nanoparticles by Tungsten Doping for Efficient and Selective Hydrogenation of Quinolines under Mild Conditions, ACS Catal. 11 (2021) 8197–8210.
[20] C. Wang, H. Wang, R. Luo, C. Liu, J. Li, X. Sun, J. Shen, W. Han, L. Wang, Metal-organic framework one-dimensional fibers as efficient catalysts for activating peroxymonosulfate, Chem. Eng. J. 330 (2017) 262–271.
[21] C.-H. Wu, W.-C. Yun, T. Wi-Afedzi, K.-Y.-A. Lin, ZIF-67 supported on marcoscale resin as an efficient and convenient heterogeneous catalyst for Oxone activation, J. Colloid Interface Sci. 514 (2018) 262–271.
[22] L. Peng, X. Gong, X. Wang, Z. Yang, Y. Liu, In situ growth of ZIF-67 on a nickel foam as a three-dimensional heterogeneous catalyst for peroxymonosulfate activation, RSC Adv. 8 (46) (2018) 26377–26382.
[23] M.J. Foysal, R. Fotedar, C.-Y. Tay, S.K. Gupta, Biological filters regulate water quality, modulate health status, immune indices and gut microbiota of freshwater crayfish, marron (Cherax cainii, Austin, 2002), Chemosphere 247 (2020), 125821.
[24] M.A.N. Khan, P.K. Klu, C. Wang, W. Zhang, R. Luo, M. Zhang, J. Qi, X. Sun, L. Wang, J. Li, Metal-organic framework-derived hollow Co_3O_4/carbon as efficient catalyst for peroxymonosulfate activation, Chem. Eng. J. 363 (2019) 234–246.
[25] M. Zhang, C. Xiao, X. Yan, S. Chen, C. Wang, R. Luo, J. Qi, X. Sun, L. Wang, J. Li, Efficient removal of organic pollutants by metal–organic framework derived Co/C yolk–shell nanoreactors: size-exclusion and confinement effect, Environ. Sci. Technol. 54 (16) (2020) 10289–10300.
[26] J. Cao, Z. Yang, W. Xiong, Y. Zhou, Y. Wu, M. Jia, S. Sun, C. Zhou, Y. Zhang, R. Zhong, Peroxymonosulfate activation of magnetic Co nanoparticles relative to an N-doped porous carbon under confinement: Boosting stability and performance, Sep. Purif. Technol. 250 (2020), 117237.
[27] H. Yong, X. Wei, J. Hu, Z. Yuan, S. Guo, D. Zhao, Y. Zhang, Hydrogen storage behavior of Mg-based alloy catalyzed by carbon-cobalt composites, J. Magnes. Alloy. 9 (6) (2021) 1977–1988.
[28] Q. Ran, X. Wang, P. Ling, P. Yan, J. Xu, L. Jiang, Y. Wang, S. Su, S. Hu, J. Xiang, A thermal-assisted electrochemical strategy to synthesize carbon dots with bimodal photoluminescence emission, Carbon 193 (2022) 404–411.
[29] C. Feng, Y. Guo, S. Qiao, Y. Xie, L.i. Zhang, L. Zhang, W. Wang, J. Wang, 2-Methylimidazole as a nitrogen source assisted synthesis of a nano-rod-shaped Fe/

FeN@N-C catalyst with plentiful FeN active sites and enhanced ORR activity, Appl. Surf. Sci. 533 (2020), 147481.
[30] G. Zhan, H.C. Zeng, ZIF-67-Derived Nanoreactors for Controlling Product Selectivity in CO_2 Hydrogenation, ACS Catal. 7 (11) (2017) 7509–7519.
[31] X.-D. Du, C.-C. Wang, J.-G. Liu, X.-D. Zhao, J. Zhong, Y.-X. Li, J. Li, P. Wang, Extensive and selective adsorption of ZIF-67 towards organic dyes: Performance and mechanism, J. Colloid Interface Sci. 506 (2017) 437–441.
[32] R. Ranjithkumar, P. Lakshmanan, P. Devendran, N. Nallamuthu, S. Sudhahar, M. K. Kumar, Investigations on effect of graphitic carbon nitride loading on the properties and electrochemical performance of g-C_3N_4/TiO_2 nanocomposites for energy storage device applications, Mater. Sci. Semicond. Process. 121 (2021), 105328.
[33] G. Yang, Q. Gao, S. Yang, S. Yin, X. Cai, X. Yu, S. Zhang, Y. Fang, Strong adsorption of tetracycline hydrochloride on magnetic carbon-coated cobalt oxide nanoparticles, Chemosphere 239 (2020), 124831.
[34] Y. Yang, G. Banerjee, G.W. Brudvig, J.-H. Kim, J.J. Pignatello, Oxidation of Organic Compounds in Water by Unactivated Peroxymonosulfate, Environ. Sci. Technol. 52 (2018) 5911–5919.
[35] B. Liu, Y. Li, Y. Wu, S. Xing, Enhanced degradation of ofloxacin by persulfate activation with Mn doped CuO: Synergetic effect between adsorption and non-radical activation, Chem. Eng. J. 417 (2021), 127972.
[36] F.-X. Wang, C.-C. Wang, X. Du, Y. Li, F. Wang, P. Wang, Efficient removal of emerging organic contaminants via photo-Fenton process over micron-sized Fe-MOF sheet, Chem. Eng. J. 429 (2022), 132495.
[37] Y.-H. Guan, J. Ma, Y.-M. Ren, Y.-L. Liu, J.-Y. Xiao, L.-Q. Lin, C. Zhang, Efficient degradation of atrazine by magnetic porous copper ferrite catalyzed peroxymonosulfate oxidation via the formation of hydroxyl and sulfate radicals, Water Res. 47 (2013) 5431–5438.
[38] X. He, K.E. O'Shea, Selective oxidation of H1-antihistamines by unactivated peroxymonosulfate (PMS): Influence of inorganic anions and organic compounds, Water Res. 186 (2020), 116401.
[39] M. Peters, Q. Guo, H. Strauss, R. Wei, S. Li, F. Yue, Contamination patterns in river water from rural Beijing: A hydrochemical and multiple stable isotope study, Sci. Total Environ. 654 (2019) 226–236.
[40] J. Lee, U. von Gunten, J.-H. Kim, Persulfate-Based Advanced Oxidation: Critical Assessment of Opportunities and Roadblocks, Environ. Sci. Technol. 54 (2020) 3064–3081.
[41] X.-D. Du, X.-H. Yi, P. Wang, W. Zheng, J. Deng, C.-C. Wang, Robust photocatalytic reduction of Cr(VI) on UiO-66-NH_2(Zr/Hf) metal-organic framework membrane under sunlight irradiation, Chem. Eng. J. 356 (2019) 393–399.
[42] X. Zhou, Q. Zhao, J. Wang, Z. Chen, Z. Chen, Nonradical oxidation processes in PMS-based heterogeneous catalytic system: Generation, identification, oxidation characteristics, challenges response and application prospects, Chem. Eng. J. 410 (2021), 128312.
[43] M. Li, S. You, X. Duan, Y. Liu, Selective formation of reactive oxygen species in peroxymonosulfate activation by metal-organic framework-derived membranes: A defect engineering-dependent study, Appl. Catal. B Environ. 312 (2022), 121419.
[44] J. Kim, T. Zhang, W. Liu, P. Du, J.T. Dobson, C.-H. Huang, Advanced oxidation process with peracetic acid and Fe(II) for contaminant degradation, Environ. Sci. Technol. 53 (2019) 13312–13322.
[45] Y. Wang, D. Cao, M. Liu, X. Zhao, Insights into heterogeneous catalytic activation of peroxymonosulfate by Pd/g-C_3N_4: The role of superoxide radical and singlet oxygen, Catal. Commun. 102 (2017) 85–88.
[46] L. Wang, X.u. Lan, W. Peng, Z. Wang, Uncertainty and misinterpretation over identification, quantification and transformation of reactive species generated in catalytic oxidation processes: A review, J. Hazard. Mater. 408 (2021), 124436.
[47] P. Hong, Z. Wu, D. Yang, K. Zhang, J. He, Y. Li, C. Xie, W. Yang, Y. Yang, L. Kong, J. Liu, Efficient generation of singlet oxygen ($^1O_2$) by hollow amorphous Co/C composites for selective degradation of oxytetracycline via Fenton-like process, Chem. Eng. J. 421 (2021), 129594.
[48] W. Wang, X. Li, F. Deng, J. Liu, X. Gao, J. Huang, J. Xu, Z. Feng, Z. Chen, L. Han, Novel organic/inorganic PDI-Urea/BiOBr S-scheme heterojunction for improved photocatalytic antibiotic degradation and H_2O_2 production, Chin. Chem. Lett. (2022), https://doi.org/10.1016/j.cclet.2022.01.058.
[49] X.-W. Zhang, F. Wang, C.-C. Wang, P. Wang, H. Fu, C. Zhao, Photocatalysis activation of peroxodisulfate over the supported Fe_3O_4 catalyst derived from MIL-88A(Fe) for efficient tetracycline hydrochloride degradation, Chem. Eng. J. 426 (2021), 131927.
[50] L. Tang, Y. Liu, J. Wang, G. Zeng, Y. Deng, H. Dong, H. Feng, J. Wang, B. Peng, Enhanced activation process of persulfate by mesoporous carbon for degradation of aqueous organic pollutants: Electron transfer mechanism, Appl. Catal. B Environ. 231 (2018) 1–10.
[51] J. Yu, L. Tang, Y. Pang, G. Zeng, H. Feng, J. Zou, J. Wang, C. Feng, X. Zhu, X. Ouyang, J. Tan, Hierarchical porous biochar from shrimp shell for persulfate activation: A two-electron transfer path and key impact factors, Appl. Catal. B Environ. 260 (2020), 118160.
[52] H. Zhou, D. He, A.I. Saana, J. Yang, Z. Wang, J. Zhang, Q. Liang, S. Yuan, J. Zhu, S. Mu, Mesoporous-silica induced doped carbon nanotube growth from metal–organic frameworks, Nanoscale 10 (2018) 6147–6154.
[53] H.B. Aiyappa, J. Thote, D.B. Shinde, R. Banerjee, S. Kurungot, Cobalt-modified covalent organic framework as a robust water oxidation electrocatalyst, Chem. Mater. 28 (2016) 4375–4379.
[54] F. Wang, H. Fu, F.-X. Wang, X.-W. Zhang, P. Wang, C. Zhao, C.-C. Wang, Enhanced catalytic sulfamethoxazole degradation via peroxymonosulfate activation over amorphous CoSx@SiO_2 nanocages derived from ZIF-67, J. Hazard. Mater. 423 (2022), 126998.
[55] Y. Liu, X. Chen, Y. Yang, Y. Feng, D. Wu, S. Mao, Activation of persulfate with metal–organic framework-derived nitrogen-doped porous Co@C nanoboxes for highly efficient p-Chloroaniline removal, Chem. Eng. J. 358 (2019) 408–418.
[56] X. Duan, Z. Ao, H. Sun, S. Indrawirawan, Y. Wang, J. Kang, F. Liang, Z.H. Zhu, S. Wang, Nitrogen-Doped Graphene for Generation and Evolution of Reactive Radicals by Metal-Free Catalysis, ACS Appl. Mater. Interfaces 7 (7) (2015) 4169–4178.
[57] H. Luo, X. Zhou, Q. Chen, J. Zhou, Removal of 2,4-dichlorophenoxyacetic acid by the boron-nitrogen Co-doped carbon nanotubes: Insights into peroxymonosulfate adsorption and activation, Sep. Purif. Technol. 259 (2021), 118196.
[58] S. Zhang, H. Gao, X. Xu, R. Cao, H. Yang, X. Xu, J. Li, MOF-derived CoN/N-C@SiO_2 yolk-shell nanoreactor with dual active sites for highly efficient catalytic advanced oxidation processes, Chem. Eng. J. 381 (2020), 122670.
[59] Y. Liu, H. Zou, H. Ma, J. Ko, W. Sun, K. Andrew Lin, S. Zhan, H. Wang, Highly efficient activation of peroxymonosulfate by MOF-derived CoP/CoO_x heterostructured nanoparticles for the degradation of tetracycline, Chem. Eng. J. 430 (2022), 132816.
[60] J.-S. Wang, X.-H. Yi, X. Xu, H. Ji, A.M. Alanazi, C.-C. Wang, C. Zhao, Y.V. Kaneti, P. Wang, W. Liu, Y. Yamauchi, Eliminating tetracycline antibiotics matrix via photoactivated sulfate radical-based advanced oxidation process over the immobilized MIL-88A: Batch and continuous experiments, Chem. Eng. J. 431 (2022), 133213.
[61] H. Demir-Duz, O. Ayyildiz, A.S. Aktürk, M.G. Álvarez, S. Contreras, Approaching zero discharge concept in refineries by solar-assisted photo-Fenton and photo-catalysis processes, Appl. Catal. B Environ. 248 (2019) 341–348.
[62] M. Li, M. Hao, L. Yang, H. Yao, J.R. Bolton, E.R. Blatchley, Z. Qiang, Trace Organic Pollutant Removal by VUV/UV/chlorine Process: Feasibility Investigation for Drinking Water Treatment on a Mini-Fluidic VUV/UV Photoreaction System and a Pilot Photoreactor, Environ. Sci. Technol. 52 (2018) 7426–7433.
[63] F.J. Beltrán, F.J. Rivas, R. Montero-de-Espinosa, Ozone-enhanced oxidation of oxalic acid in water with cobalt catalysts. 1. Homogeneous catalytic ozonation, Ind. Eng. Chem. Res. 42 (2003) 3210–3217.
[64] S. Li, J. Huang, X. Li, L. Li, The relation of interface electron transfer and PMS activation by the H-bonding interaction between composite metal and MCM-48 during sulfamethazine ozonation, Chem. Eng. J. 398 (2020), 125529.
[65] M. Mahdi-Ahmed, S. Chiron, Ciprofloxacin oxidation by UV-C activated peroxymonosulfate in wastewater, J. Hazard. Mater. 265 (2014) 41–46.
[66] M. Tichonovas, E. Krugly, D. Jankunaite, V. Racys, D. Martuzevicius, Ozone-UV-catalysis based advanced oxidation process for wastewater treatment, Environ. Sci. Pollut. Res. 24 (2017) 17584–17597.
[67] H. Chen, Z. Zhang, D. Hu, C. Chen, Y. Zhang, S. He, J. Wang, Catalytic ozonation of norfloxacin using Co_3O_4/C composite derived from ZIF-67 as catalyst, Chemosphere 265 (2021), 129047.
[68] D. Miklos, W.-L. Wang, K. Linden, J. Drewes, U. Hübner, Comparison of UV-AOPs (UV/H_2O_2, UV/PDS and UV/Chlorine) for TOrC removal from municipal wastewater effluent and optical surrogate model evaluation, Chem. Eng. J. 362 (2019) 537–547.
[69] X.-H. Yi, T.-Y. Wang, H.-Y. Chu, Y. Gao, C.-C. Wang, Y.-J. Li, L. Chen, P. Wang, H. Fu, C. Zhao, W. Liu, Effective elimination of tetracycline antibiotics via photoactivated SR-AOP over vivianite: A new application approach of phosphorus recovery product from WWTP, Chem. Eng. J. 449 (2022), 137784.